Verification of experimental dynamic strength methods with atomistic ramp-release simulations

Alexander P. Moore, Justin L. Brown, Hojun Lim, and J. Matthew D. Lane

Sandia National Laboratories, Albuquerque, New Mexico 87185, USA

Material strength and moduli can be determined from dynamic high-pressure ramp-release experiments using an indirect method of Lagrangian wave profile analysis of surface velocities. This method, termed self-consistent Lagrangian analysis (SCLA), has been difficult to calibrate and corroborate with other experimental methods. Using nonequilibrium molecular dynamics, we validate the SCLA technique by demonstrating that it accurately predicts the same bulk modulus, shear modulus, and strength as those calculated from the full stress tensor data, especially where strain rate induced relaxation effects and wave attenuation are small. We show here that introducing a hold in the loading profile at peak pressure gives improved accuracy in the shear moduli and relaxation-adjusted strength by reducing the effect of wave attenuation. When rate-dependent effects coupled with wave attenuation are large, we find that Lagrangian analysis overpredicts the maximum unload wavespeed, leading to increased error in the measured dynamic shear modulus. These simulations provide insight into the definition of dynamic strength, as well as a plausible explanation for experimental disagreement in reported dynamic strength values.

I. INTRODUCTION

Material strength is a broadly applied and critically important measure, yet its exact definition can depend on whether one is dealing with brittle or ductile matter, or whether a material is deformed quickly or slowly. Fundamentally, strength is a material's ability to resist permanent deformation. However, quantifying this physical concept has become increasingly difficult as experiments delve into ever higher pressures, faster strain rates, and novel materials, which exhibit unusual failure and plastic mechanisms.

Dynamic compression is an important tool to reach pressures much higher than can currently be achieved through quasistatic loading. Understanding the problems of material response at extreme pressures is important to fields as diverse as geomorphology [1], armoring [2], advanced materials manufacturing [3,4], and fusion energy [5]. In each, our goal is to measure and understand the mechanisms that determine strength in dynamic compression.

At low stress and strain rates, there are many conventional experimental techniques available to determine deformation mechanisms [6–8], strength [9–13], and elastic moduli [14–17], but as the strain rate increases, the experimental analysis techniques become very limited. This has led to an incomplete understanding of the dynamic material response in these high-pressure regimes. Recent experiments have applied the theory of high-rate deformation mechanisms [18] to extract strength. One method uses Rayleigh-Taylor instability growth as a gauge of strength [19], while other methods use one-dimensional (1D) wave propagation combined with either diffraction measurement [20] or known equations of state (EOS) [21]. Alternatively, in ramp-release experiments [22–27], properties such as strength, bulk modulus, and shear modulus are obtained without prior knowledge of the material EOS. These experiments use velocimetry at specified locations and a previously established self-consistent Lagrangian

analysis (SCLA) method [28]. Using SCLA, Brown *et al.* [23] have recently obtained strength and shear modulus values at 250 GPa for Ta well above those predicted by previous models, which raised questions about the applicability of SCLA in this regime. Here, we validate the SCLA methodology using molecular dynamics (MD) at the same pressure as experiment.

In this paper, we use MD simulations to validate the dynamic strength and material moduli extracted with SCLA, and to identify SCLA limitations. We directly test fundamental wave propagation assumptions necessary for valid strength extraction. We apply wave scaling arguments to identify rate-dependent processes, and we use Lagrangian analysis of atomistic velocity histories to compare dynamic high strain-rate analysis with the atomistic stress tensor. No assumptions are made about the deformation mechanisms, which allow this atomistic-to-continuum wave technique to be extended to a host of materials, such as metals, ceramics, polymers, and glasses. Our analysis here is on body-centered-cubic (bcc) tantalum, which has important applications in the extreme environments community [29,30]. More broadly, our results offer much needed confirmation of a key methodology for measurement of high-pressure dynamic strength. Such confirmation and increased understanding will lead to the development of improved experimental methodology for strength extraction—a critical step toward a more complete understanding of the physical mechanisms (i.e., plasticity, etc.) in extreme environments. Here we present one such methodology for obtaining improved shear moduli and relaxation-adjusted strength.

II. METHODOLOGY

MD simulations solve the classical equations of motion for the atoms in the system, and the particle velocities and stresses can be directly obtained for multiple locations along

the wave propagation direction, allowing velocimetry analysis to be applied without the experimental difficulty of window corrections. In experiments, the back surface measurement is convoluted by the sample and window impedance mismatch, requiring additional corrections. The MD simulations of wave evolution can be scaled and compared to experiments due to the invariance of the particle velocity, stress, density, and strain [31]. The MD simulations' per-atom stress and velocity information, along with the ability to control the compression profile, is used to validate and understand the SCLA extracted material properties.

SCLA is an analysis technique that examines the deviatoric response from unloading a plastically deformed state and allows strength and elastic moduli to be extracted at pressures above the elastic-plastic transition. SCLA methodology is discussed elsewhere [22,23] and is briefly summarized here. The analysis requires velocity-time histories from two (or more) positions within a sample. Assuming isentropic flow of forward propagating simple waves [32], where X and t represent Lagrangian space and time, the wavespeed (c) can be calculated as a function of particle velocity (u) using Eq. (1),

$$c_u = (\partial X/\partial t)_u = \left(\frac{\Delta X}{\Delta t}\right)_u. \tag{1}$$

Assuming a homogeneous medium with only one-dimensional uniaxial strain wave propagation, the stress balance, conservation of mass, and momentum give

$$\sigma_x = P + \frac{4}{3}\tau, \; d\sigma_x = \rho_0 c(u)du, \; d\varepsilon = \frac{du}{c(u)}, \tag{2}$$

where ρ_0 is the initial density, ε is the strain, P is the pressure, τ is the resolved shear stress ($\frac{1}{2}[\sigma_x - \sigma_t]$), σ_t is the transverse stress ($[\sigma_y + \sigma_z]/2$), and σ_x is the longitudinal stress.

Equation (2) can be rearranged to obtain the change in longitudinal stress as a function of wavespeed and strain from the conservation equations and substituted into the stress balance equation differentiated with respect to strain to obtain the Lagrangian bulk velocity $c_B = \sqrt{\frac{1}{\rho_0}(\frac{dP}{d\varepsilon})}$, which represents the wavespeed in completely plastic regions, and the longitudinal unloading wavespeed $c_L = \sqrt{\frac{1}{\rho_0}(\frac{dP}{d\varepsilon} + \frac{4}{3}\frac{d\tau}{d\varepsilon})}$, which represents the wavespeed in the elastic and quasielastic regions. The wavespeed velocities can then be used to extract the bulk modulus (K) and shear modulus (G) at the maximum particle velocity (u_{max}) directly from their definitions,

$$K = \rho_0(1 - \varepsilon_{max})c_B^2(u_{max}), \tag{3}$$

$$G = \rho_0(1 - \varepsilon_{max})\sqrt{\frac{3}{4}\left[c_L^2(u_{max}) - c_B^2(u_{max})\right]}. \tag{4}$$

We note that this type of shear modulus extraction assumes purely elastic behavior immediately after maximum particle velocity (equivalently maximum pressure). Moving beyond just examination of the peak wavespeeds, Eq. (2) can be integrated between the regions of c_L and c_B to determine the change in shear stress over this elastic to plastic transition,

$$\tau(u_1) - \tau(u_2) = \frac{3}{4}\rho_0 \int_{u_2}^{u_1} \left[c_L^2(u) - c_B^2(u)\right]\frac{du}{c(u)}. \tag{5}$$

The change in shear stress from Eq. (5) during unloading is often related to the flow strength [25–27]. For our discussion, here we will equate $Y_{SCLA} = \Delta\tau = \tau(u_1) - \tau(u_2)$, which is valid for either the von Mises or Tresca yield criterion under simple uniaxial strain. Attenuation correction factors are applied to G and Y_{SCLA} when necessary [22,23].

We used the classical MD code, LAMMPS [33], with the embedded-atom method potential Ta1 by Ravelo *et al.* [34]. Nanocrystalline systems were constructed by Voronoi tessellation, then annealed to relax grain junctions. Details have been previously published [31]. The system unit cell was 19.73 nm × 19.73 nm × 131.4 nm with 3 million atoms, had grain sizes ranging from 1.4 to 13.5 nm with 6 nm average, and a density of 16.58 g/cm^3. The system was equilibrated in an isothermal-isobaric (NPT) ensemble to relax surfaces and system volume followed by a microcanonical (NVE) ensemble with a Langevin thermostat. The integration time step was 0.2 fs and the system was equilibrated at 300 K and 0 GPa.

Quasistatic simulations of homogeneous deformation were performed as a reference against which to compare the dynamic bulk and shear moduli results. Quasistatic simulations at nonzero temperature and pressure were achieved by deforming the preequilibrated system in an NVE ensemble, and the statistical average change in the stress tensor is examined, allowing the elastic constants to be calculated [35].

Propagating ramp compression waves were imposed with a moving infinite-mass momentum mirror piston. The periodic polycrystal was replicated in the direction of the wave propagation, resulting in simulations between 12 and 45 million atoms. To apply SCLA to the ramp wave history, atoms were mapped to material points (MP) and tracked throughout the course of the simulation. Figure 1 depicts the motion and tracking of MPs as the compression wave propagates though the system, visualized using OVITO [36]. MPs were placed every 25 nm along the propagation direction. The MP thickness of 0.4 nm was chosen to be large enough to give a good statistical representation of the atoms in different grain orientations, but small enough to capture the wave features. The average velocity and per-atom stresses in the MPs were calculated at each time step. High-temperature liquid simulations were performed to verify that MP diffusion did not influence analysis.

The MD simulations were performed with two distinct loading profiles to investigate wave effects on the extracted dynamic properties: ramp-release and ramp-hold-release. A cubic polynomial was used to specify the load and unload piston velocity profiles as in Lane *et al.* [31] to suppress shock-up. The ramp-release profile is similar to traditional experimental profiles, where the compression ramp-up is immediately followed by a ramp-down, as shown in Fig. 1. The ramp-hold-release profile was performed with the same ramp and release rates, but with a 5 ps hold at the maximum particle velocity. This delays wave attenuation by separating compression and rarefaction waves. 5 ps is sufficient to observe relaxation in our nanocrystalline Ta (see below). The piston loading and unloading time was set to 80 and 30 ps, respectively, resulting in a $5 \times 10^9/1.33 \times 10^{10}$ s^{-1} average loading/unloading rate.

The SCLA method was applied to two MD velocity histories, resulting in the Lagrangian wavespeed as a function of particle velocity; an example is shown in Fig. 2. The dynamic
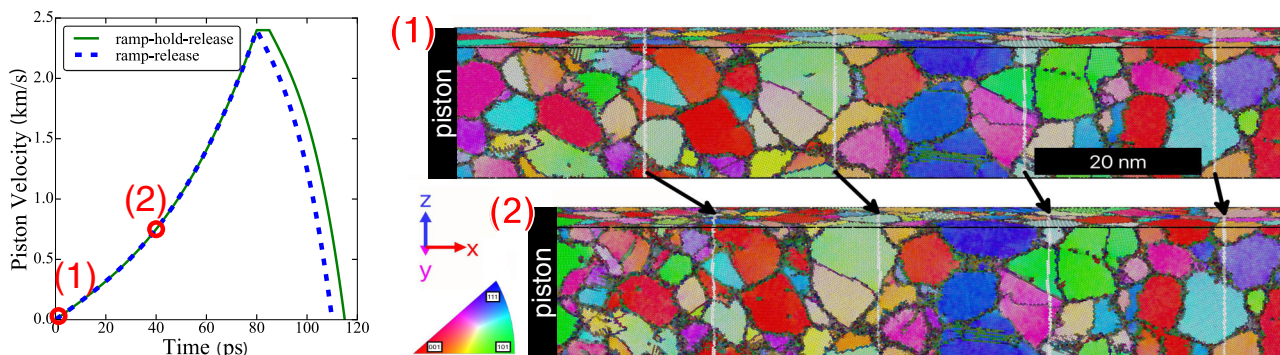
FIG. 1. Snapshots of nanocrystalline Ta compression at two points in time. The atoms are colored by crystal orientation, with darker intensity indicating low-confidence regions (i.e., grain boundaries and defects). Arrows depict Lagrangian material point (MP) movement.

strength, bulk modulus, and shear modulus can then be extracted from the atomistic simulations using the same methods, described by Eqs. (3)–(5), as in experiments. The ramp-release and ramp-hold-release profiles show nearly identical loading wavespeeds for particle velocities below 2.3 km/s, but they show marked differences near the peak particle velocities. The ramp-release profile has a significantly larger unloading wavespeed $c_L(u_{max})$, while the ramp-hold-release profile has a dip in Lagrangian wavespeed below the linear loading fit.

Propagating the peak wavespeeds through Eqs. (3) and (4) results in SCLA estimates of the bulk and shear moduli. These estimates are not local properties, but are averaged between the MPs used. By repetition across several MP ranges (from 0 to 100 nm), the mean and standard deviation of the bulk and shear moduli can be obtained.

III. RESULTS AND DISCUSSION

We test the accuracy of the dynamic SCLA bulk and shear moduli by comparing against the quasistatic MD values at 250 GPa, shown in Table I. The quasistatic simulations were performed at 1200 K to match the dynamic simulation's temperature just before unloading. Excellent agreement between the SCLA and quasistatic moduli is obtained for all

simulations, except the shear modulus in the ramp-release case. By varying the hold time in the ramp-hold-release runs, we are able to show shear modulus convergence.

Given the precision of the bulk modulus calculation, the source of error in the SCLA shear modulus is the error in $c_L(u_{max})$. As shown in Fig. 2, this velocity is significantly higher in the ramp-release analysis. Past experiments have reported high $c_L(u_{max})$ values, and attributed these to wave attenuation effects [26,27]. However, because the variation in the SCLA shear modulus across the different MPs (and thus different levels of attenuation) cannot explain the observed errors, attenuation alone is not a sufficient explanation. To examine the role of rate dependence near peak particle velocities, and its possible effect on the errors in peak wavespeed, a second set of simulations were conducted with double the loading and unloading rates. These simulations were scaled as in [31], and they are compared to the original lower rate simulations in Fig. 3, where we focus on the regions near the peak particle velocity, to which this SCLA method is particularly sensitive. There is insignificant rate dependence where the scaled profiles overlay. As illustrated, the ramp-release simulations exhibit significant rate dependence at the peak velocity, while the ramp-hold-release simulations do not. We conclude that the artificially high $c_L(u_{max})$ is due to a combination of rate dependencies and wave attenuation effects.

We test the accuracy of the dynamic SCLA strength by comparing it to the atomistic stress tensor. Integrating the wavespeed profiles with Eq. (5) (represented by the shaded regions in Fig. 2) results in the SCLA extracted strength (Y_{SCLA}) for both MD simulations. These results are compared directly to the true MD strength ($\Delta\tau$) extracted from
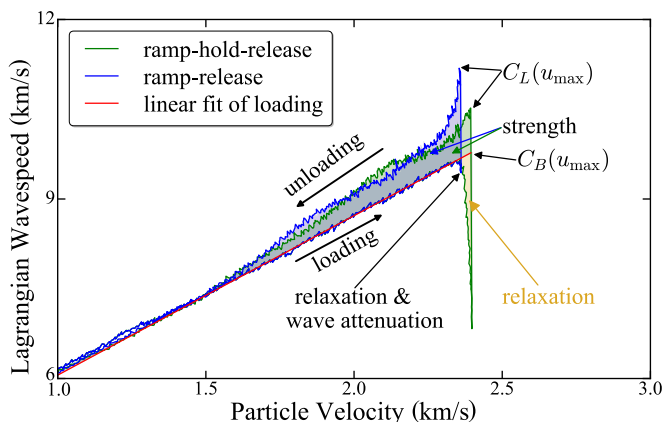

FIG. 2. MD Lagrangian wavespeed vs particle velocity obtained using SCLA on the 0–100 nm MPs comparing the ramp-hold-release vs ramp-release simulations. Relaxation, strength, and important wavespeed definitions are illustrated.

TABLE I. Comparison of bulk and shear moduli at 250 GPa and 1200 K for the quasistatic MD and SCLA extracted values.

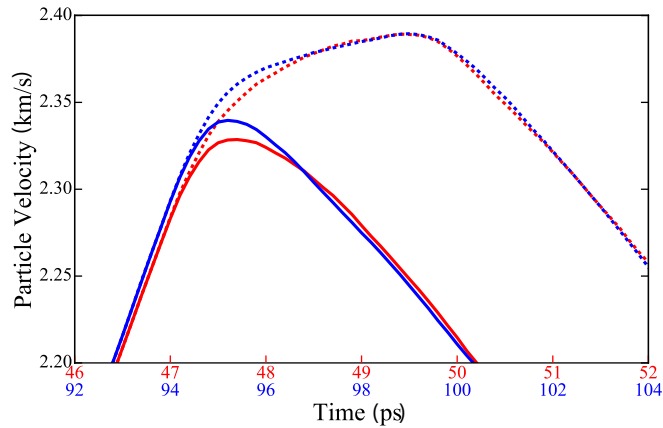|	Bulk mod. (GPa)	Shear mod. (GPa)
Quasistatic MD	951.5	128.0
Ramp-hold(5 ps)-release	953.8 ± 0.7	129.4 ± 2.4
Ramp-hold(4 ps)-release	954.0 ± 1.8	132.5 ± 9.0
Ramp-hold(3 ps)-release	954.9 ± 1.7	150.9 ± 19.0
Ramp-hold(2 ps)-release	953.4 ± 1.3	180.2 ± 22.1
Ramp-release	948.3 ± 1.4	251.3 ± 30.3

FIG. 3. Two particle velocity histories from 75 nm (red) and 150 nm (blue) Lagrangian MPs with the faster and original loading/unloading rates, respectively, scaled and overlaid, for both the ramp-release (solid) and ramp-hold-release (dashed) simulations. Rate-dependent regions are where the profiles do not overlay.

FIG. 5. Normal stress components and shear stress (τ) vs time for the ramp-release and ramp-hold-release 50 nm Lagrangian MP. The $\Delta\tau$ that contributes to SCLA strength is illustrated.

the per-atom stress tensor versus pressure path in Fig. 4. We find that the SCLA definition of strength is equal to the average total change in shear stress τ from the peak pressure to the minimum τ during unloading. The average here is over the space through which the wave has propagated. The calculated SCLA strength (represented by the magnitude of the vertical lines in Fig. 4) differs between the ramp-hold-release and the ramp-release by exactly the shear stress relaxation at peak pressure observed in the ramp-hold-release simulations. This indicates that SCLA strength is sensitive to the compression profile, particularly near peak pressure. This is a clear indication of path dependence. The sensitivity to compression profiles provides a plausible explanation for the experimental variations in reported strength. Note that in both cases the SCLA extracted strength is consistent with the MD stress tensor value—a further validation of the method.

To further explore relaxation and how it contributes to path-dependent extracted strength, we compare MP stress histories for the two different compression profiles in Fig. 5.
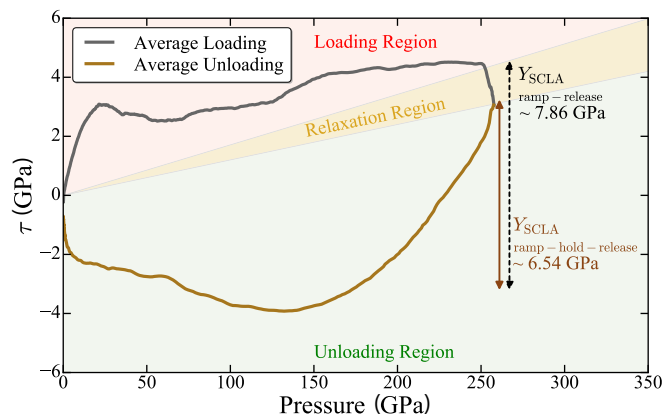

FIG. 4. The average shear stress (τ) between 0 and 100 nm MPs vs pressure, illustrating the average unloading $\Delta\tau$ equating to the SCLA extracted strengths.
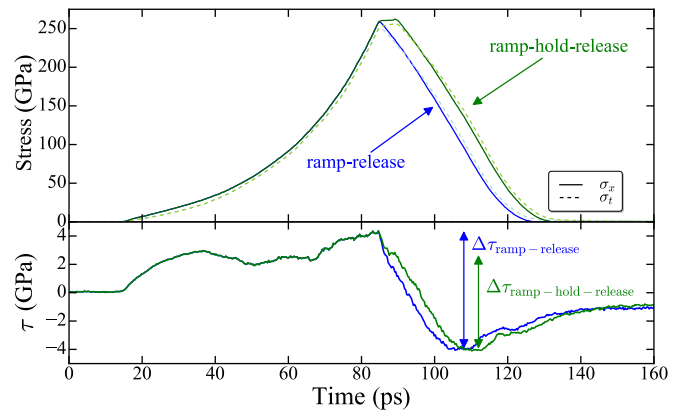
The rapid change in strain rate between the ramp and hold in the ramp-hold-release case leads to a lowering of the yield shear stress, which causes τ to relax over time before unloading. Conversely, in the ramp-release case, the immediate reversal of the applied loading does not give the material an opportunity to relax before unloading. This causes the change in shear stress from relaxation to be incorporated into the ramp-release SCLA extracted strength as depicted in Fig. 5. These histories illustrate how relaxation affects the SCLA strength by demonstrating the $\Delta\tau$ that contributes to SCLA strength.

Materials with rate-dependent deformation exhibit relaxation [37], whose rate is governed by its relaxation mechanisms. In our nanocrystalline simulations, the majority of relaxation is due to shear stress migration to grain boundaries followed by grain boundary relaxation occurring over picosecond time scales. Relaxation in polycrystalline metals is likely dominated by dislocation motion [38], which has slower relaxation times causing relaxation to be present in slower strain rate ramp-release paths, as shown by previous stress relaxation tests [39,40] and shock rise times [38,41]. The resulting relaxation times in ramp-hold-release experiments presents a method for deciphering relaxation mechanisms.

Our work can be generalized to experiments, even to those with different relaxation mechanisms and much longer relaxation times than we can explore with molecular simulations. We have shown that the reliability of SCLA measurements can be significantly improved when an extended flat-top hold separates the ramp from the release wave. In experiments, where a perfect flat-top hold can be challenging to implement, an approximate hold (i.e., significantly reduced ramp-rate region) should be sufficient to delay interaction between ramp and release response, and thereby reduce wave attenuation. By comparing the SCLA results in experiments with and without holds, one can test for and eliminate the effects of decreased shear stress due to strain-rate-induced relaxation and obtain a new relaxation-adjusted strength measurement.

IV. CONCLUSIONS

In conclusion, we have directly validated self-consistent Lagrangian analysis methods by application to fully atomistic propagating ramp waves combined with an atomistic Lagrangian analysis technique. Our validation of the dynamic strength extraction will likely prompt significant investigation into new high pressure strength models, which are needed to reconcile the observed increase in strength over previously accepted models. The SCLA extracted strength agrees with the change in shear stress τ determined from the MD stress tensor. Moreover, we show where limitations exist when significant rate-dependent effects and wave attenuation are present. We show that these limitations can be avoided by incorporating sufficient hold times at peak pressure. We observe that strength is influenced by the loading profile, and we argue that careful control of the profile and hold duration could be used to obtain a relaxation-adjusted strength measurement. Rate effects at peak pressure were found to explain the artificially high $c_L(u_{max})$ values that cause the large discrepancies in shear modulus at high pressures. Our results indicate the importance of shaping the compression profiles in experimental applications of SCLA for shear modulus and strength.

[1] R. Hemley, P. Bell, and H. Mao, Science **237**, 605 (1987).

[2] L. S. Magness, Mech. Mater. **17**, 147 (1994).

[3] H.-C. Kim, D.-Y. Oh, and I.-J. Shon, Int. J. Refract. Met. Hard Mater. **22**, 197 (2004).

[4] M. A. Meyers, B. B. Gupta, and L. E. Murr, JOM **33**, 21 (1981).

[5] J. Lindl, Phys. Plasmas **2**, 3933 (1995).

[6] C. Ruestes, E. Bringa, R. Rudd, B. Remington, T. Remington, and M. Meyers, Sci. Rep. **5**, 16892 (2015).

[7] W. Johnston and J. J. Gilman, J. Appl. Phys. **30**, 129 (1959).

[8] M.-C. Miguel, A. Vespignani, S. Zapperi, J. Weiss, and J.-R. Grasso, Nature (London) **410**, 667 (2001).

[9] C. Lee, X. Wei, J. W. Kysar, and J. Hone, Science **321**, 385 (2008).

[10] J. R. Cahoon, W. H. Broughton, and A. R. Kutzak, Metall. Trans. **2**, 1979 (1971).

[11] E. Broch and J. Franklin, in *International Journal of Rock Mechanics and Mining Sciences & Geomechanics Abstracts* (Elsevier, Amsterdam, 1972), Vol. 9, pp. 669–676.

[12] E. Orowan, Rep. Prog. Phys. **12**, 185 (1949).

[13] S. W. Tsai and E. M. Wu, J. Compos. Mater. **5**, 58 (1971).

[14] W. C. Oliver and G. M. Pharr, J. Mater. Res. **7**, 1564 (1992).

[15] Z. Hashin, *The Elastic Moduli of Heterogeneous Materials* (U.S. Department of Commerce, Office of Technical Services, Washington, D.C., 1960).

[16] D. S. Hughes and J. Kelly, Phys. Rev. **92**, 1145 (1953).

[17] A. Bosak, M. Krisch, M. Mohr, J. Maultzsch, and C. Thomsen, Phys. Rev. B **75**, 153408 (2007).

[18] M. A. Meyers, *Dynamic Behavior of Materials* (Wiley, New York, 1994).

[19] H.-S. Park, R. Rudd, R. Cavallo, N. Barton, A. Arsenlis, J. Belof, K. Blobaum, B. El-dasher, J. Florando, C. Huntington *et al.*, Phys. Rev. Lett. **114**, 065502 (2015).

[20] A. Comley, B. Maddox, R. Rudd, S. Prisbrey, J. Hawreliak, D. Orlikowski, S. Peterson, J. Satcher, A. Elsholz, H.-S. Park *et al.*, Phys. Rev. Lett. **110**, 115501 (2013).

[21] D. K. Bradley, J. H. Eggert, R. F. Smith, S. T. Prisbrey, D. G. Hicks, D. G. Braun, J. Biener, A. V. Hamza, R. E. Rudd, and G. W. Collins, Phys. Rev. Lett. **102**, 075503 (2009).

[22] J. L. Brown, C. S. Alexander, J. R. Asay, T. J. Vogler, and J. L. Ding, J. Appl. Phys. **114**, 223518 (2013).

[23] J. L. Brown, C. S. Alexander, J. R. Asay, T. J. Vogler, D. H. Dolan, and J. L. Belof, J. Appl. Phys. **115**, 043530 (2014).

[24] J. L. Brown, M. D. Knudson, C. S. Alexander, and J. R. Asay, J. Appl. Phys. **116**, 033502 (2014).

[25] J. R. Asay, T. Ao, J.-P. Davis, C. Hall, T. J. Vogler, and G. T. Gray, J. Appl. Phys. **103**, 083514 (2008).

[26] J. R. Asay, T. Ao, T. J. Vogler, J.-P. Davis, and G. T. Gray, J. Appl. Phys. **106**, 073515 (2009).

[27] T. Vogler, T. Ao, and J. Asay, Int. J. Plast. **25**, 671 (2009), Special Issue in Honor of Dattatraya (Datta) Dandekar.

[28] J. Asay and J. Lipkin, J. Appl. Phys. **49**, 4242 (1978).

[29] R. W. Buckman, JOM **52**, 40 (2000).

[30] S. Cardonne, P. Kumar, C. Michaluk, and H. Schwartz, Int. J. Refract. Met. Hard Mater. **13**, 187 (1995).

[31] J. M. D. Lane, S. M. Foiles, H. Lim, and J. L. Brown, Phys. Rev. B **94**, 064301 (2016).

[32] D. S. Drumheller, *Introduction to Wave Propagation in Nonlinear Fluids and Solids* (Cambridge University Press, Cambridge, 1998).

[33] S. Plimpton, J. Comput. Phys. **117**, 1 (1995), LAMMPS website: http://lammps.sandia.gov.

[34] R. Ravelo, T. C. Germann, O. Guerrero, Q. An, and B. L. Holian, Phys. Rev. B **88**, 134101 (2013).

[35] T. Kraft, P. M. Marcus, M. Methfessel, and M. Scheffler, Phys. Rev. B **48**, 5886 (1993).

[36] A. Stukowski, Modell. Simul. Mater. Sci. Eng. **18**, 015012 (2009).

[37] P. Perzyna, Adv. Appl. Mech. **9**, 243 (1966).

[38] J. Winey, J. Johnson, and Y. Gupta, J. Appl. Phys. **112**, 093509 (2012).

[39] I. Gupta and J. C. Li, Metall. Mater. Trans. B **1**, 2323 (1970).

[40] H. M. Musal, in *Laser Induced Damage in Optical Materials: 1979*, Vol. 568, edited by H. E. Bennett, A. J. Glass, A. H. Guenther, and B. E. Newman (National Bureau of Standards, 1980).

[41] L. C. Chhabildas and J. R. Asay, J. Appl. Phys. **50**, 2749 (1979).